

# Analysis of Flow and Thermal Performance of SiO<sub>2</sub>- Water Nanofluids with Variable Geometrical and Process Parameters

N. Oumer<sup>#1\*</sup>, H. Wan Azmi<sup>#1</sup>, Azizuddin Abd Aziz<sup>#2</sup>, J. P. Siregar<sup>#1</sup>, Aklilu T. Baheta<sup>#2</sup>

<sup>1</sup>Faculty of Mechanical and Automotive Engineering Technology, Universiti Malaysia Pahang, 26600, Pekan, Pahang, Malaysia

<sup>2</sup>College of Electrical and Mechanical Engineering Department, Sustainable Energy Centre of Excellence, Addis Ababa Science and Technology University, 16417, Addis Ababa, Ethiopia

\*e-mail: [nurye@ump.edu.my](mailto:nurye@ump.edu.my)

## Article Info

**Page Number:** 6416-6435

**Publication Issue:**

**Vol. 71 No. 4 (2022)**

## Article History

**Article Received:** 25 March 2022

**Revised:** 30 April 2022

**Accepted:** 15 June 2022

## Abstract

This study numerically investigated the thermal-hydraulic performances of a single-phase SiO<sub>2</sub>-water nanofluid in forced convective turbulent flow in a pipe. The nanoparticle volume concentrations varied from 0-4% by weight. At different *Re*s, bulk temperatures, and particle sizes, simulations were run. The obtained results showed that, in comparison to other input parameters, nanoparticle concentration and inlet velocity considerably affect the heat transfer coefficient (*h*) and pressure drop ( $\Delta p$ ). The analysis of thermal and flow performance discovered that increasing the nanoparticle concentration and inflow velocity significantly improves the ( $\Delta p$  and *h*).

**Keywords:** simulation modelling; heat transfer; nanofluids; CFD; nanoparticles

---

## Introduction

A nanofluid can be defined as a combination of solid nanoparticles and a liquid base-fluid with at least one of the principal dimensions of the nanoparticles being less than 100 nanometers. They are prepared by the distribution of nanoparticles in a base-fluid. When the nanoparticle is combined with the base-fluid, the thermal conductivity (*k*) of the fluid is enhanced and improves its capability of energy exchange.

Nanofluids are known for their enhanced thermal properties and can primarily be used as industrial coolants. They can also be used as smart fluids (in the area of cell phones and laptops), and as combustion heat enhancers in diesel engines [1-5]. In the application of such fluids in energy systems, the top priority investigations being done are in the areas of heat exchangers, heat pumps, energy conversion and storage devices [6-7]. For instance, a car cooling system applies the concept of heat transfer; if the heat is not released to the surrounding, the car will overheat and it will damage the car engine and its accessories such as gaskets, sealing of the oil gallery, and water jacket. Hence, a thorough understanding of the enhancement of heat transfer rate using nanofluids is important to ensure that the heat can be released quickly and efficiently. The nanoparticles that are commonly used for nanofluid preparation include Silicon dioxide (SiO<sub>2</sub>), Titanium dioxide (TiO<sub>2</sub>), Copper (II) oxide (CuO), Zinc oxide (ZnO), and Aluminium oxide (Al<sub>2</sub>O<sub>3</sub>), while the base-fluid can be water, ethylene

glycol, and a mixture of the two base-fluids. Due to their enhanced thermal-hydraulic properties, the base-fluids: ethylene glycol, water, and oil are significantly dominant in the preparation of nanofluids over the other base-fluids [8-11].

The primary determinants of heat transfer efficiency are the thermal and physical characteristics of nanofluids, including their viscosity, density, specific heat capacity, and thermal conductivity. The thermal performances and fluid dynamics of nanofluids are highly dependent on their thermophysical properties while the thermophysical properties are dependent on volumetric concentration, temperature, and the dispersed nanoparticles. Various research works have been conducted on the investigation of the thermal and physical properties of various nanofluids under different working conditions. For instance, Tadepalli et al. [12] characterized the thermal and physical properties of various nanoparticles at cryogenic temperatures. They found that, at 3% particle concentration, the effective density increases as the temperature increases for all nanoparticles. They observed a similar pattern for other volume concentrations as well. Additionally, it was shown that viscosity for all nanoparticles decreased with temperature rise whereas it increased with volume fraction at a certain temperature. It is also found that for SiO<sub>2</sub> nanofluid, the specific heat of the nanofluid increased with the decrease in the nanoparticle volume concentration, [12]. In addition, the viscosity and thermal conductivity of nanofluids increased with increasing the concentration of nanoparticles as reported by Logesh et al. [13] for the case of silicon oxide (SiO<sub>2</sub>) suspended in water with different volume fractions.

Most of the existing research studies for the application of nanofluids in heat transfer are by using the experimental method [14-18]. However, an experimental investigation is expensive and time-consuming. Moreover, in almost all applications, it is difficult to visualize the flow and thermal phenomena inside the domain where the nanofluids flow [19]. For this, a numerical simulation is an ideal tool. Many researchers have examined the thermal-hydraulic performance of various nanofluids using either in-house code or commercial software. Li et al. [20] studied the thermal-hydraulic behavior of Cu-water nanofluid flow in a trapezoidal microchannel by using ANSYS CFX-10 software. They found that, with only a slight increase in pressure drop, the Cu-water nanofluids considerably improved the thermal performance of the microchannel mixture flow, which in turn increased the pumping power. Particularly, the volume fraction boosts thermal performance. In another study, Bianco et al. [21] numerically studied the hydrodynamic and thermal behaviors of Al<sub>2</sub>O<sub>3</sub>-water nanofluids in a circular tube with a constant heat flux at the wall surface. Fluent was used as the computational fluid dynamic software to solve the governing and other related equations. According to the numerical findings, the nanoparticle contributed to the improvement of heat transfer compared to the base-fluid. In both single-phase and two-phase models, the maximum average  $h$  difference between them was 11%.

The effectiveness of a counter-flow rectangular microchannel heat exchanger (MCHE) using water-based CuO, Ag, SiO<sub>2</sub>, TiO<sub>2</sub>, and Al<sub>2</sub>O<sub>3</sub> nanofluids for high volume concentrations (2%–10%) was examined in numerical analysis by Mohammad et al. [22]. The three-dimensional steady and laminar flow in the aluminum MCHE was simulated using the finite volume approach. Their findings demonstrated that the addition of nanoparticles raised the bulk

temperature of the cold fluids, which improved heat transmission. The SiO<sub>2</sub>-water nanofluid exhibited the maximum  $h$ , pressure drop, shear stress, and pumping power, whereas the Ag-water nanofluid had the highest total bulk temperature. Through the use of CFD modeling of a horizontal circular tube, Moghadassi et al. [23] recently examined the impact of nanofluids on laminar forced convective heat transport. With a mean particle size of 15 nm and a volume concentration of 0.1%, water-based Al<sub>2</sub>O<sub>3</sub> and Al<sub>2</sub>O<sub>3</sub>-Cu hybrid nanofluids were employed. Additionally, models with one and two phases were taken into consideration. The outcomes showed that the friction factor and  $\Delta p$  increased with the inclusion of nanoparticles. Additionally, a modest amount of Cu nanoparticles added to the base-fluids increased heat transmission by around 5% and the two-phase technique is more accurate than the single-phase model.

To the authors' best knowledge there are few numerical studies of the thermal-hydraulic performance of SiO<sub>2</sub>-water nanofluids. Even these studies are either for laminar flow or very high particle concentrations. Moreover, there is no study conducted to predict the optimum combinations of geometrical parameters (such as the diameter of the tube and size of the particles) and process parameters (such as the inlet velocity, flow rate, inlet temperature, heat flux, and nanoparticle concentration) for maximum heat transfer with a minimal  $\Delta p$  penalty.

The lack of numerical studies involving a turbulent flow of SiO<sub>2</sub>-water nanofluids at low volume concentration inspired the current investigation. The fluid flow fields, thermal, and performance characteristics of a forced convection flow of SiO<sub>2</sub>-water nanofluid at various geometrical and process parameters are investigated using a numerical simulation approach. The results are discussed in the form of the pressure drop, temperature profile, pumping power  $h$ , of the circular tube.

#### *Thermal and Physical Properties*

The thermophysical properties of the SiO<sub>2</sub>-water nanofluids at various concentrations were obtained by using mathematical equations and from previous experimental data done by one of the authors of this paper. The specific heat capacity and density of the nanofluids obtained from Eqns (1) and (2) respectively.

$$\rho_{nf} = \phi\rho_p + (1 - \phi)\rho_w \quad (1)$$

$$C_{nf} = \frac{\phi(\rho c)_p + (1 - \phi)(\rho c)_w}{\phi\rho_p + (1 - \phi)\rho_w} \quad (2)$$

where  $\phi$  is the volume fraction of the nanoparticle,  $\rho$  is the density,  $C$  is the specific heat capacity, and the subscripts  $nf$ ,  $p$ , and  $w$  represent the nanofluid, nanoparticle, and water respectively.

The viscosity and thermal conductivity of the SiO<sub>2</sub>-nanofluids at each particle concentration were determined using the mathematical relations developed by Sharma et al. [24] which are valid for particle concentration  $\phi \leq 4\%$ ; nanofluid temperature  $T_{nf} \leq 70^\circ C$  and particle diameter  $d_p \leq 170nm$ .

$$\frac{\mu_{nf}}{\mu_w} = \left(1 - \frac{\phi}{100}\right)^{11.3} \left(1 + \frac{T_{nf}}{70}\right)^{-0.038} \left(1 + \frac{d_p}{170}\right)^{-0.061} \quad (3)$$

$$\frac{k_{nf}}{k_w} = 0.8938 \left(1 - \frac{\phi}{100}\right)^{1.37} \left(1 + \frac{T_{nf}}{70}\right)^{0.2777} \left(1 + \frac{d_p}{150}\right)^{-0.0336} \left(\frac{\alpha_p}{\alpha_w}\right)^{-0.01737} \quad (4)$$

Where  $\mu$  is the viscosity,  $k$  is the thermal conductivity, and  $\alpha$  is the thermal diffusivity.

All the aforementioned thermal and physical properties were combined in the current study to investigate the thermal-hydraulic performance of SiO<sub>2</sub>-water nanofluids at various particle concentrations are summarized in Table 1 for the case where the inlet temperature is 30 °C and the nanoparticles diameter is 22 nm. The viscosity effect on the pumping power and heat transfer is more profound compared to other thermophysical properties [25, 26]. All the thermophysical properties show changes with concentration.

Table 1. Thermal and physical properties of the nanofluids at an inlet temperature of 30 °C.

Volume Conc., (%)	Density, (kg/m <sup>3</sup> )	Heat capacity, (J/kg.K)	Thermal conductivity (W/kg.K)	Viscosity, (Pa.s)
0	995.7	4178.40	0.6154	0.000798
0.005	1001.82	4140.36	0.627413	0.000827
0.01	1007.94	4102.78	0.631694	0.000874
0.015	1014.07	4065.65	0.635982	0.000925
0.02	1020.19	4028.97	0.640278	0.000977
0.025	1026.31	3992.73	0.644582	0.001033
0.03	1032.43	3956.92	0.648893	0.001091
0.035	1038.55	3921.53	0.653212	0.001153
0.04	1044.67	3886.55	0.65754	0.001217
0.045	1050.79	3851.98	0.661874	0.001285
0.05	1056.92	3817.82	0.666217	0.001356

### Experimental Data for Model Validation

The experimental measurements of the  $\Delta p$  and  $h$  for the numerical model validations were done by one of the authors of this paper. Figure 1 depicts the experimental setup. The test section is a 1.5-long circular copper pipe with  $D_{out} = 0.019$  m and  $D_{in} = 0.016$  m respectively. It was

enclosed with heating coils. In addition to the test section, other connecting pipes with variable diameters were used to connect the test section with other components such as the tank, chiller, pump and flow meter. The overall length of the piping system was approximately 4 m. The length of the tube leading to the test section inlet is kept at an appropriate length to so that the fluid enters the pipe in a turbulent state. The nanofluids were collected in a 30-liter tank and forced to circulate in the system using a 0.5 HP pump.

1500-Watt rating nichrome heaters were used as a heating source by wrapping them around the pipe's outer surfaces. To eliminate the heat-loss, the pipe was insulated with ceramic fiber. Multiple *K*-type thermocouples were attached (as shown in Fig. 1) to collect temperature data. The nanofluid was pre-heated with a constant input of 600 Watt while the nanofluid leaving the test section was further cooled down up to 30 °C using a chiller for all cases. The  $\Delta p$  was measured using a pressure transducer. The steady-state nature of the experiment was determined by recording the temperatures (both the surface and bulk temperatures using a data logger every 5 seconds. Flow rate, temperatures, and power input to the heater were recorded under steady-state conditions. The experiments were carried out with SiO<sub>2</sub> nanoparticle concentrations between 0% and 4% at different flow rate values.

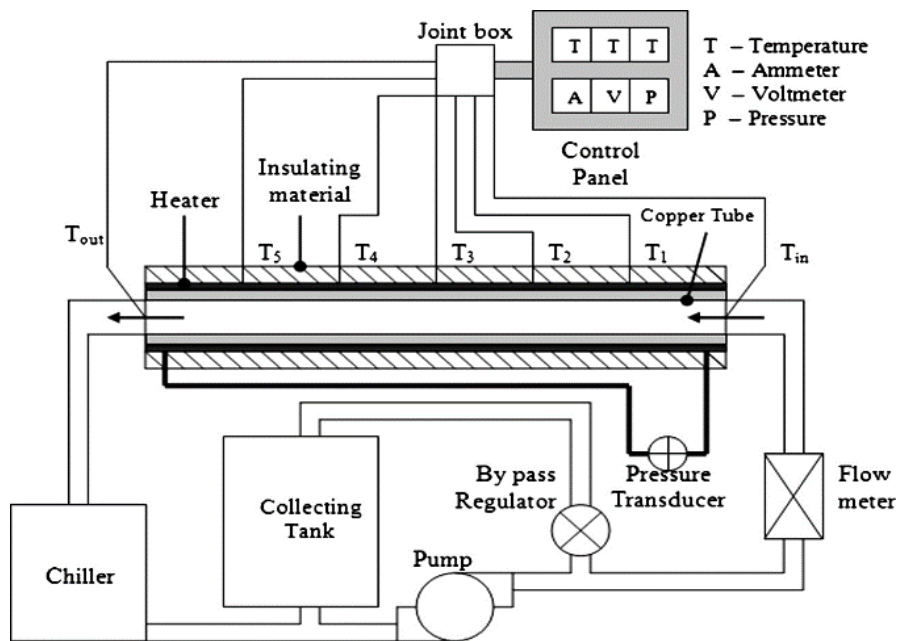


**Fig. 1: schematic diagram of the expertimental setup**

## Mathematical Modeling

### *Computational domain and governing equations*

The axial velocity and temperature of the nanofluid are both uniform when it enters the tube. Since the circular tube cross-section is symmetrical, only one-quarter of the circle is used in the computation with the use of symmetry boundary conditions. The test section with the boundary names used in the numerical simulation is shown in Fig. 2.

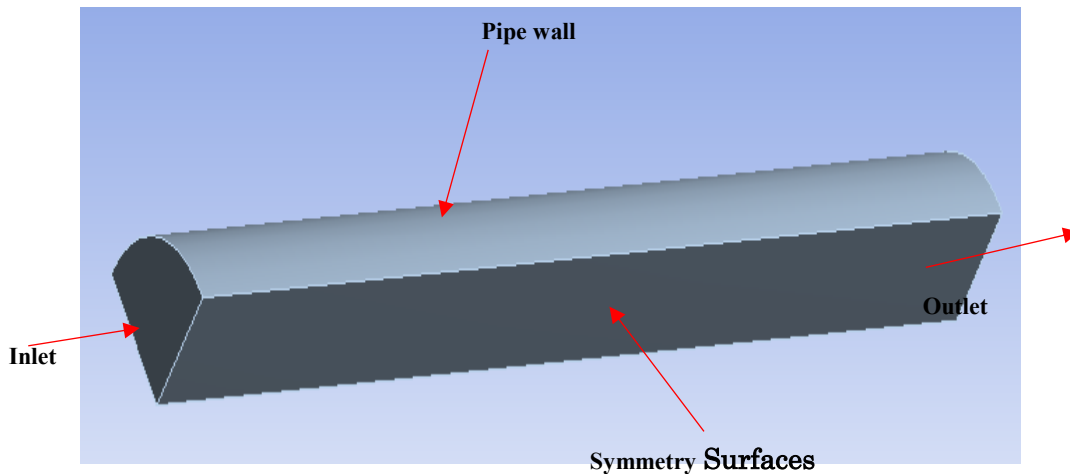


Fig. 2: The computational domain used in the present analysis

According to the experimental findings of Pak and Cho [27], it is presumable that the SiO<sub>2</sub> nanoparticles in the water are easily fluidized, and as a result, the SiO<sub>2</sub>-water nanofluid behaves like a single-phase fluid. Furthermore, because nanoparticles are substantially smaller than microparticles in size and therefore have a reduced relative velocity, it is assumed that the base-fluid and the nanoparticles are thermally in an equilibrium condition with zero relative velocity. The effective thermal and physical qualities depend on temperature and particle concentration, as shown in Eqns. (3) and (4). Ansys Fluent software is used to solve the flow and energy governing equations, as well as the turbulent transport equations, based on these assumptions. The continuity, momentum, and energy governing equations are:

$$\frac{\partial \bar{u}_i}{\partial x_i} = 0 \quad (5)$$

$$\rho \frac{\partial (\overline{u_i u_j})}{\partial x_i} = -\frac{\partial \bar{p}}{\partial x_j} + \mu \frac{\partial^2 \bar{u}_j}{\partial x_i^2} + \rho \frac{\partial (\overline{u_i' u_j'})}{\partial x_i} \quad (6)$$

$$\frac{\partial (\overline{u_i T})}{\partial x_i} = \frac{k}{\rho C_p} \frac{\partial^2 \bar{T}}{\partial x_i^2} - \frac{\partial (\overline{u_i' T'})}{\partial x_i} \quad (7)$$

Where  $\bar{u}$ ,  $\bar{p}$ , and  $\bar{T}$ , respectively, are the time-averaged velocity, pressure, and temperature, while the subscripts  $i$  and  $j$  represent coordinate axes. The terms  $u'$  and  $T'$  are the velocity and temperature fluctuations, respectively, while  $\overline{u_i' u_j'}$  and  $\overline{u_i' T'}$  being turbulent shear stress and turbulent heat flux. In this study, the well-known  $k-\varepsilon$  turbulent model is used.

**Boundary conditions and numerical procedure**

The flow and energy governing equations together with the turbulent equations outlined from Eqs. (5) to (9) are non-linear partial differential and coupled equations. Before the equations are solved using a numerical method, the equations need to be discretized to a system of linear algebraic equations and solved using the iteration procedure. For this, the equations are subjected to certain boundary conditions. Due to the symmetry nature of the tube, only one-quarter of the tube was modelled. Table 2 provides the boundary conditions employed in the current simulation..

Table 2. The boundary condition of the simulation model

At the tube inlet section	<ul style="list-style-type: none"> <li>- Uniform axial velocity <math>V_{in}</math> and temperature <math>T_{in}</math> have been specified.</li> <li>- <math>V_{in} = 0.5 \text{ m/s} - 2 \text{ m/s}</math>, <math>T_{in} = 303 \text{ K}</math></li> </ul>
At the outlet section	<ul style="list-style-type: none"> <li>- Outflow boundary condition has been implemented for the outlet section. This boundary condition implies zero normal gradients for all flow variables except pressure.</li> <li>- Gauge pressure, <math>P_{out} = 0 \text{ Pa}</math></li> <li>- Backflow temperature = 300 K</li> </ul>
At the top wall	<ul style="list-style-type: none"> <li>- On the upper wall of the tube, the no-slip boundary condition was imposed. The wall is subjected to a uniform heat flux which is similar to the heat flux used in the experiment.</li> <li>- Constant Heat flux, <math>q = 7957.75 \text{ W/m}^2</math></li> </ul>
At the symmetry surfaces	<ul style="list-style-type: none"> <li>- On the sidewalls of the modelled domain, the symmetry boundary condition was applied. In the present analysis, the near-wall treatment was based on enhanced wall functions</li> </ul>

Ansys Fluent 17.2 was employed to solve the fluid flow and heat transfer problems. The governing equations are discretized by ANSYS Fluent using the finite volume method, which results in a set of linear algebraic equations. The convection and diffusion terms were discretized using the 2<sup>nd</sup> order upwind approach. The SIMPLE technique was employed to solve the coupled pressure and velocity equations [25].

**Mesh-independency test**

To make sure that the generated results are not varying with different grid sizes, a mesh independence test was performed. In this research, three-dimensional and unstructured (non-uniform) grids are generated with various grid sizes. Moreover, to consider the effect of the tube walls on the flow and heat transfer, the grids near the tube surfaces were made finer compared to the grids at the centre of the tube. A total of six different mesh sizes namely: 20000, 50000, 70000, 90000, 110000, and 130000 were used for the mesh independence test.

Fig.3 shows the variation of  $h$  against different element sizes for different concentrations of nanoparticles when the  $Re$  is 13000. The  $h$  slightly increases from element size 20000 to 70000 at all concentrations, as shown in the figure. Though there are changes in heat transfer values,

the maximum percentage change between different element sizes is only 4.59 %. Hence, it can be concluded from the results that any mesh size can be employed for the heat transfer analysis.

Similarly, as depicted in Fig.4, the  $\Delta p$  variation against different grid sizes for different nanoparticle concentrations when the  $Re$  is 4000. Unlike the heat transfer results, the  $\Delta p$  results show a slight increment of  $\Delta p$  from 20000 to 130000 at all concentrations. However, the increment is so small that the maximum percentage of increment is 3.45 %. Thus, any mesh size can be selected to analyze the pressure drop. Therefore, in this research, the 20000-element size was selected for the analysis.

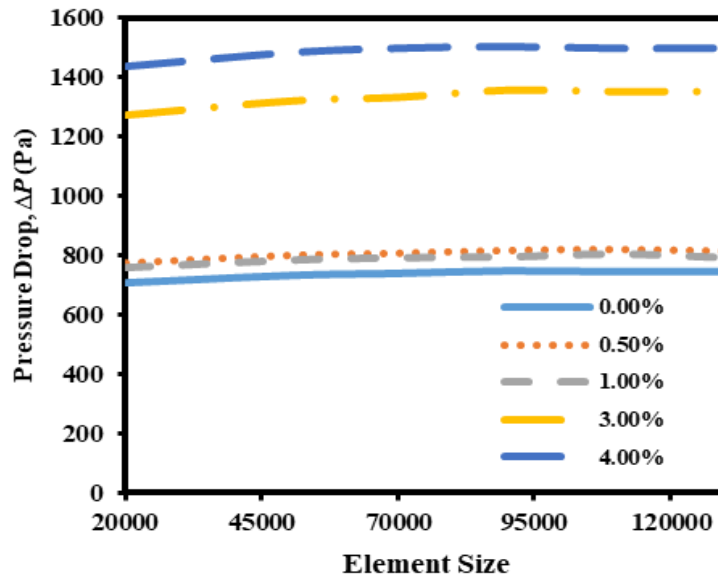


Fig. 3: Results of  $\Delta p$  vs element size at various concentrations.

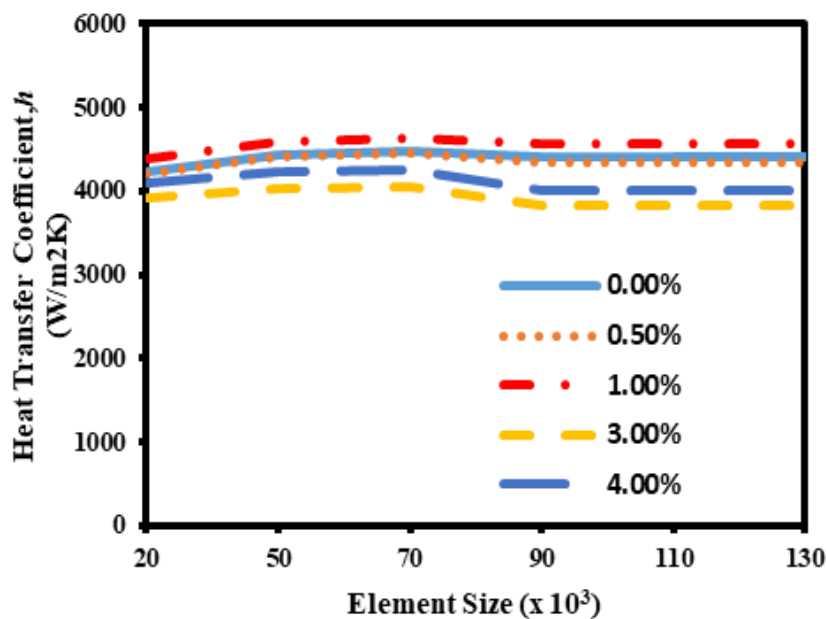


Fig. 4: Results of  $h$  vs element size at different concentrations.

## Results and Discussions

### Validation

Before a detailed analysis of the  $\Delta p$  and heat transfer characteristics of SiO<sub>2</sub>-water nanofluids in circular tubes, the developed numerical model should be checked for accuracy. For this, the heat transfers and  $\Delta p$  results found using the current approach are compared with experimental data obtained from literature and with standard empirical equations. The validation of the heat transfer performance found from the current numerical investigation is compared with the data done by the third author of this paper (Azim et al. [28]) for the same flow and geometric parameters. Fig.5 shows the variation of  $h$  against Re at various concentrations. The concentration of nanofluids that are selected for the validation are 0.0% (pure water), 0.5%, 1.0% and 3.0%. As can be seen from Fig.5, the curves demonstrate an increasing trend of  $h$  with the increment of Re for all concentrations. The maximum deviation between the numerical and experimental results for 0.0%, 0.5%, 1.0% and 3.0% are 4.39%, 7.40%, 3.47% and 13.36%, respectively. The results show that the average deviation between the simulation and experimental results is below 8%. Generally, the simulation findings match up well with the experimental data as stated in several published papers where the tolerance of the average deviation of about 8% is acceptable [29-30]. Hence, the developed model may be used to forecast the heat transfer performance of nanofluids in horizontal tubes.

Besides, the heat transfer results from the current model for pure water are compared with standard empirical equations, namely Dittus and Boelter and Gnielinski. Fig.6 depicts a comparison of the Nu with the Re between the results obtained from the current simulation and the standard empirical formulae. The figure reveals that the Nusselt number from the simulation results, experimental data and standard empirical equation rise with the increment of the Re. The variation predicted by simulation is close to the result calculated by Dittus and Boelter equation, which means the simulation result is well agreed with the Dittus Boelter equation. However, the Gnielinski equation shows over-prediction of the Nu compared to the simulation and Dittus equation at a high Re.

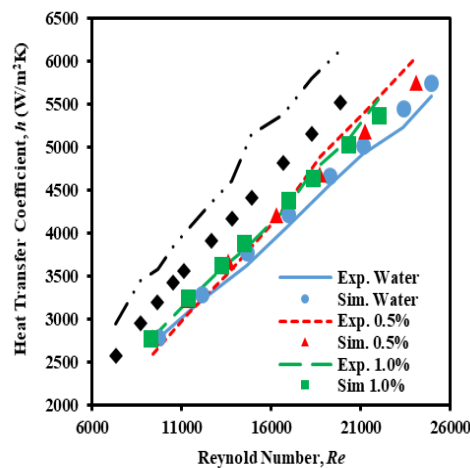


Fig. 5: Results of  $h$  at various Re values.

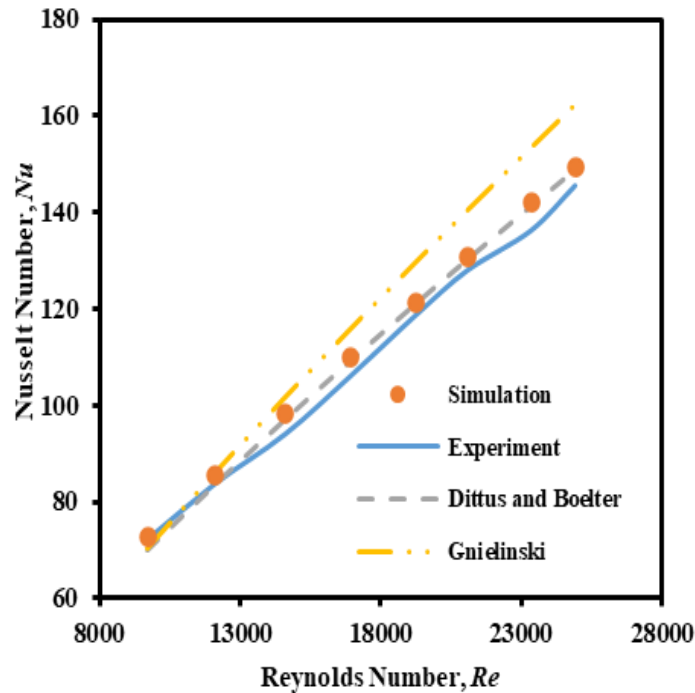


Fig. 6: Comparison of simulated results with experimental data and standard empirical results.

Similarly, the simulation results obtained from the current simulation model for flow performance are validated using the same experimental data by the third author (Azim et al. [28]). Fig.7 illustrates the variation of  $\Delta p$  at different concentrations of nanofluids with the  $Re$  at various nanofluids concentrations. The observation from the curves shows an upward trend of  $\Delta p$  when the  $Re$  is increasing for all concentrations. The average deviation of the numerical results compared to experimental data for 0.0%, 0.5%, 1.0% and 3.0% concentration of nanofluids are 10.9%, 5.7%, 11.4%, and 6.6%, respectively. It clearly depicts that the numerical findings from the current investigation are in good agreement with the experimental data since the range of deviation for most of the predicted results is within 10% of the experimental data<sup>30</sup>. The slightly higher deviations that occurred in the current analysis might be due to the value of the outlet pressure are not provided in the experimental research paper, hence the value of outlet pressure was assumed as the atmospheric pressure throughout the present research.

Furthermore, the friction factor of pure water analyzed from the current simulation is compared with the result calculated from two standard empirical equations which are Petukhov ( $f_p$ ) and Blasius ( $f_B$ ) equations. The results are presented in Fig.8. Referring to the figure, all curves display a downward trend with the increase of the  $Re$ . At a low  $Re$ , the simulation has over-predicted the friction factor compared to both standard empirical equations, however, the results are closer to the empirical results when it approaches a high  $Re$ . Hence, it can be concluded that the friction factor predicted from the simulation is acceptable since the average deviation is less than 13%. A similar deviation value has been reported as an acceptable value by the work of Xu et al<sup>31</sup>.

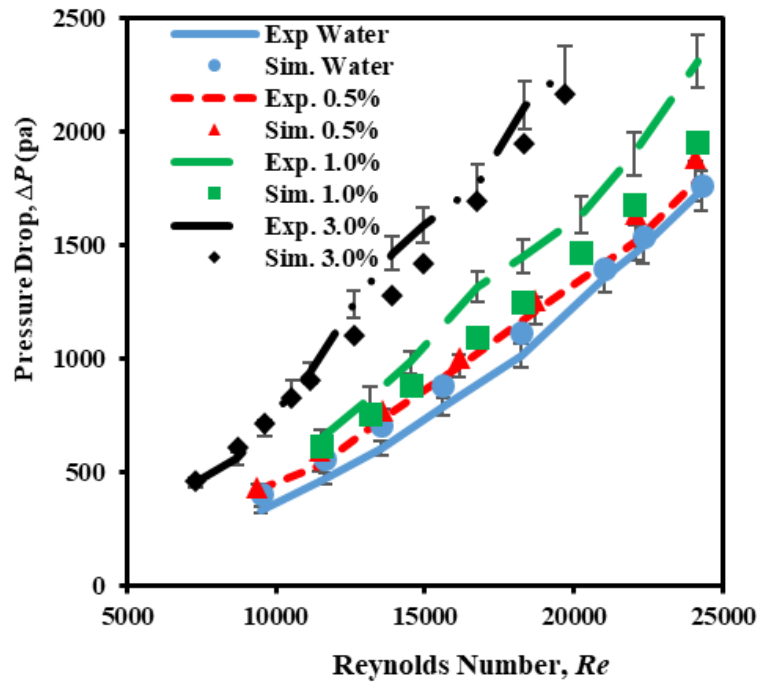


Fig. 7: Variation of  $\Delta p$  and  $Re$

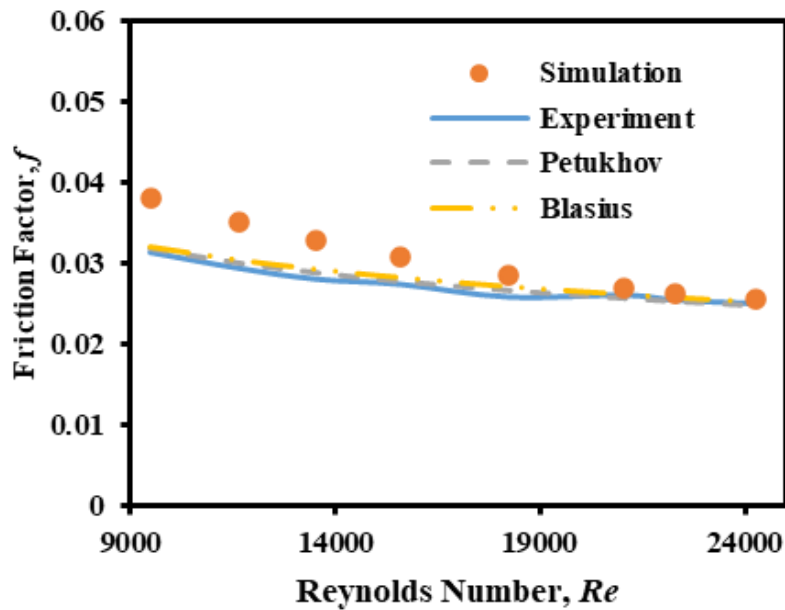


Fig. 8: Comparison of Simulated friction factor with experimental data and standard empirical result.

### *Effect of concentration of nanoparticle*

Fig. 9 shows the influence of  $\text{SiO}_2$  nanoparticle volume concentration on the  $h$  at a fixed inlet temperature of 303 K, nanoparticle size of 22 nm, and heat flux of 7957.75 W/m<sup>2</sup>. As shown in the figure, curves of 0.0%, 0.5%, 1%, 2%, 3%, and 4% nanoparticle volume concentrations present a significant increment of  $h$  with an increase in  $Re$ . For all concentrations, the average

$h$  increment from  $Re=5000$  to  $Re=25000$  is approximately 270%. This is due to the fact that fluid flowing with a high  $Re$  is constantly moving at a high speed, which causes a decrease in the thermal resistance across the boundary layer from the fluid to the heated surface. This is because fluid flowing with a high  $Re$  is always moving at high velocity, which causes a decrease in thermal resistance across the boundary layer from the fluid to the heated surface. As a result, the amount of heat that is carried away by the fluid is increased [32]. Moreover, as expected, the  $h$ s increase with the concentration of the nanoparticle. Considering the base-fluid (0% concentration) as a reference, the  $h$  enhancement by 4% volume concentration at  $Re$  of 5000 is around 21.8% while at  $Re$  of 25000, the increment of  $h$  is about 22.6%. This indicates that a higher volume concentration of nanofluids has improved the heat transfer performance. More nanoparticles are involved in the transportation of heat when a higher volume concentration is used hence the total surface area of nanoparticles is also higher thereby the performance of heat transfer is increased [33]. This is strong evidence to prove that the performance of nanofluids in heat transfer applications is more efficient than conventional fluids. High enhancement in heat transfer performance is achieved even at relatively low volume concentration.

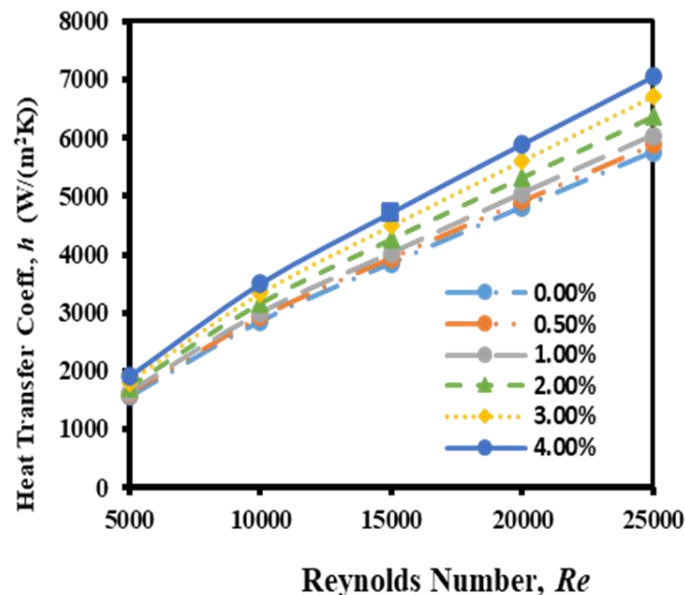


Fig. 9: Results of  $h$  vs  $Re$  at different concentration

Similarly, shown in Fig.10 is a variation of  $\Delta p$  with  $Re$  at various  $SiO_2$  nanoparticle concentrations with a fixed inlet temperature of 303 K, heat flux of 7957.75 W/m<sup>2</sup> and nanoparticle size of 22 nm. The figure shows that, at all  $Re$ s, the  $\Delta p$  increases with increasing particle concentration. At nanoparticle concentration of 4.0%, the increment of  $\Delta p$  is the most significant compared to other concentrations. A similar experimental outcome was presented by Sharma et al. for  $Al_2O_3$  nanoparticles<sup>34)</sup>. Moreover, it can be observed that the increment of  $\Delta p$  from 0% to 1% concentration is small however when the concentration is more than 1%, the  $\Delta p$  increases remarkably. For example, at  $Re$  25000, the increment of  $\Delta p$  from 0% to 1% concentration is 0.65 kPa while from 3% to 4%, the increment is 1.25 kPa. This is due to the reason that the viscosity of nanofluids increases with increasing nanoparticle concentration which intensifies the viscous sub-layer and enhances the pressure drop. However, the influence on the sub-layer at low nanoparticles concentration is small as well as the  $\Delta p$  [35].

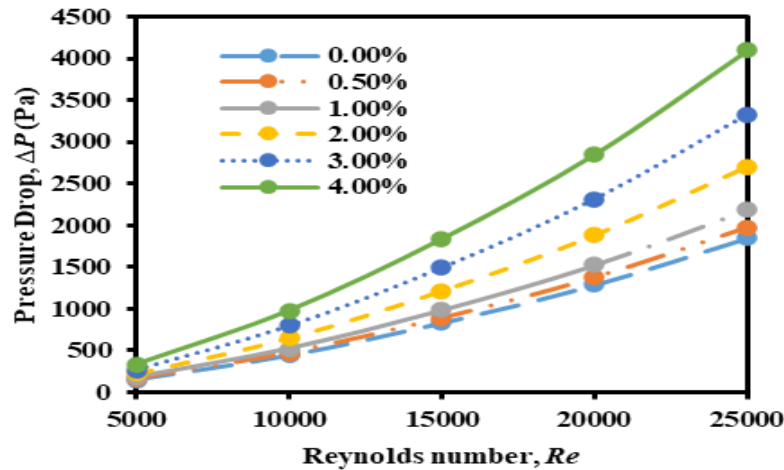


Fig. 10: Results of  $\Delta p$  and  $Re$  at different nanoparticle concentrations

**Effect of inlet temperature**

The variation of  $h$  with  $Re$  at various inlet temperatures at 3% SiO<sub>2</sub> nanoparticle concentration, heat flux of 7957.75 W/m<sup>2</sup> and nanoparticle diameter of 22 nm are displayed in Fig.11. The inlet temperatures tested in this analysis are 283 K, 293 K, 303 K, 313 K, 323 K, and 333 K. the  $h$ s of the nanofluid for all inlet temperatures show upward trends as the flow velocity increases. For instance, the increment of  $h$  from the  $Re$  of 5000 to 25000 at 283 K inlet temperatures is 270%. Besides, the numerical results also reveal that the  $h$  increases with the inlet temperature at one particular  $Re$ . For example, at 333 K and  $Re$  of 5000, the highest value of  $h$ s is found to be 1871.4 W/ m<sup>2</sup>K (6.5%) while at  $Re = 25000$  the  $h$  is 6937.12 W/ m<sup>2</sup>K (6.34%). This is because the temperature has temperature significant influent on the viscosity and thermal conductivity of the nanofluid. The viscosity of the nanofluids normally decreases with increasing of nanofluids temperature and this is similar to the trend reported by Duangthongsuk and Wongwises [36]. From the mathematical correlation presented in equation (3), the viscosity of nanofluids is directly proportional to the nanofluid temperature.

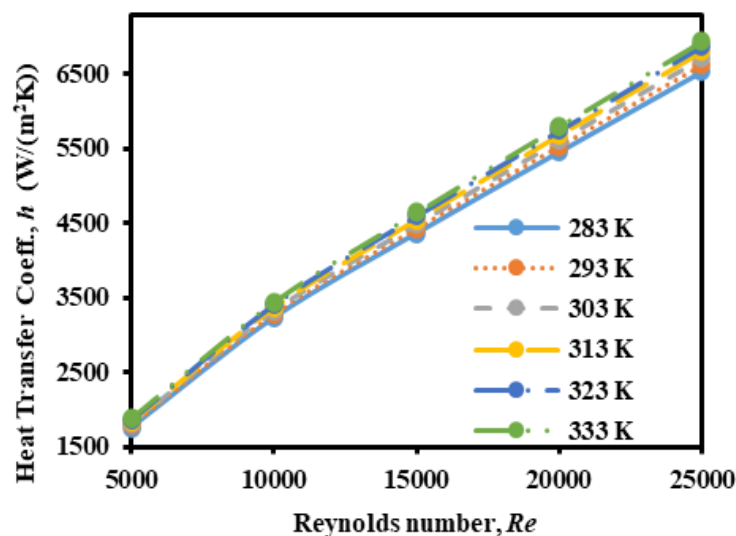


Fig. 11: Variation of  $h$  and  $Re$  at different inlet temperatures

Shown in Table 3 is the distribution of  $\Delta p$  at various inlet temperatures at 3% of nanoparticles concentration, 7597.75 W/m<sup>2</sup> of heat flux and 22.0 nm of the nanoparticle size. As expected, the  $\Delta p$  of the nanofluids at a certain inlet temperature increases exponentially as the  $Re$  increases. The average increment is around 3.05 kPa from  $Re$  of 5000 to 25000. The table also revealed that, at one specific  $Re$ , the  $\Delta p$  of the nanofluids decreases with the rising of inlet temperature. The average decrement of the  $\Delta p$  for every 10 Kelvin rises in temperature is 1% at all the  $Re$ s. As stated earlier, the temperature rise reduces the viscosity of the nanofluid due to the reduction of the binding energy of the nanoparticles and it impacts the  $\Delta p$  directly. Since the pumping power that is used to break the bonding between nanoparticles is decreased, therefore the  $\Delta p$  along the tube is also decreased.

Table 3.  $\Delta p$  at different inlet temperatures and  $Re$

Re	Pressure Drop, $\Delta P$ (Pa)					
	T <sub>in</sub> = 283	T <sub>in</sub> = 293	T <sub>in</sub> = 303	T <sub>in</sub> = 313	T <sub>in</sub> = 323	T <sub>in</sub> = 333
5000	271.8	269.3	267.19	265.3	263.5	261.9
10000	806.5	799.3	792.90	787.2	782.0	777.3
15000	1516.8	1503.2	1491.2	1480.5	1470.7	1461.8
20000	2355.4	2334.3	2315.7	2299.1	2283.9	2270.0
25000	3388.0	3357.8	3331.0	3307.0	3285.2	3265.2

### Effect of Nanoparticles Size

Table 4 displays the influence of SiO<sub>2</sub> nanoparticle sizes on the  $h$  for the case where the particle concentration and heat flux are fixed at 3% and 7597.75 W/m<sup>2</sup>, respectively. For all inlet flow velocity, the nanofluids with the lowest nanoparticle size (10 nm) have the highest  $h$  and it decreases with an increase of nanoparticle size for the same  $Re$ . As an example, the increase in the  $h$  is about 1.02 times with 10 nm SiO<sub>2</sub> nanoparticles diameter over the 100 nm diameter at all  $Re$ s. The heat transfer decrement with an increase in nanoparticle size is because the viscosity values of the 10 nm SiO<sub>2</sub> nanofluid are higher and decrease with an increase in nanoparticle size. The higher the viscosity, the higher the Prandtl number for the same concentration of SiO<sub>2</sub> nanofluids. A high Prandtl number is responsible for the higher  $h$ . A similar enhancement in  $h$  with lower particle size was observed in the works of Anoop et al. and Mirmasoumi et al.<sup>9, 37)</sup>. with the smaller size of the nanoparticle, the viscosity of SiO<sub>2</sub> nanofluids in the current analysis is improved which is the same as the behaviour presented by Jia-Fei et al.<sup>38)</sup>. Due to the presence of a higher total surface area in smaller nanoparticles, the occurrence of interface resistance with the fluid layer is increased, therefore viscosity is increased<sup>39)</sup>. At fixed  $Re$ s,  $Re= 5000$  and  $Re=25000$  for instance, the  $h$  is decreased approximately by 1.92% and 1.94%, respectively, when the particle size changes from 10 nm to 100 nm.

Table 4.  $h$  at different nanoparticle diameters and  $Re$

Nanoparticle diameter, nm	$Re = 5000$	$Re = 10000$	$Re = 15000$	$Re = 20000$	$Re = 25000$
	Heat Transfer Coefficient, $h$ ( $W/(m^2K)$ )				
10	1813.4	3333.9	4501.8	5625.2	6733.6
20	1808.7	3325.1	4489.9	5610.3	6715.8
30	1804.2	3316.8	4478.7	5596.3	6699.1
40	1800.0	3309.0	4468.1	5583.1	6683.2
50	1796.0	3301.5	4458.0	5570.5	6668.1
75	1786.7	3284.4	4434.8	5541.5	6633.5
100	1778.5	3269.1	4414.1	5515.6	6602.5

The variation of  $\Delta p$  with  $Re$  for several nanoparticles size at 3% nanoparticle concentration, 303 K inlet temperature, and 7957.75 W/m<sup>2</sup> heat flux are presented in Fig.12. The  $\Delta p$  increases exponentially with  $Re$  at constant nanoparticle size. The average increment of  $\Delta p$  from  $Re$  of 5000 to 25000 for all the nanoparticles size is approximately 3.0 kPa which is 4.83%. Furthermore, it is observed that the  $\Delta p$  slightly increases with decreasing nanoparticle diameter at constant  $Re$  and significant growth of  $\Delta p$  occurs at high  $Re$ . When the nanoparticle size increases, the overall surface tension on the surface of the SiO<sub>2</sub> nanoparticles is decreased due to the reduction of total surface area and the force of moving fluids that need to overcome the friction is reduced as well, therefore, the  $\Delta p$  along the tube is diminished. Sharma et al. [24] have found a similar behaviour for the variation of  $\Delta p$  and nanoparticle size.

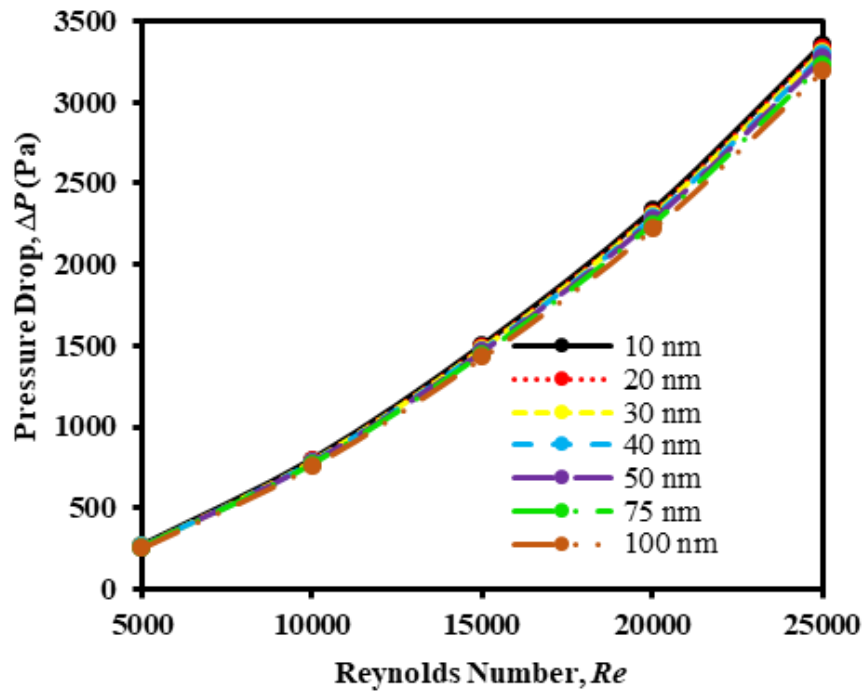


Fig. 12: Results of  $\Delta p$  and  $Re$  different nanoparticle diameter

**Effect of Heat Flux**

The last process parameter considered in the analysis is the effect of variable heat flux on heat transfer and pressure drop. Table 5 presents the  $h$  distribution with different heat fluxes and the  $Re$ . As can be seen from the table, the  $h$  increases with the increase of the  $Re$  at constant heat flux. The average increment of  $h$  from the  $Re$  of 5000 to 25000 at all heat flux is 273%. However, the  $h$  increment with increasing heat flux is insignificant. For instance, at the constant  $Re$ , when the heat flux increased from 6631.46 W/m<sup>2</sup> to 132629.12 W/m<sup>2</sup>, the  $h$  increments is only 0.03% and 0.01%, respectively. A similar observation of minimal heat transfer enhancement with heat flux was obtained in the study by Trisaksri and Wongwises [40]. Since the increment of  $h$  is insignificant with heat flux, therefore this variable can be considered constant when analyzing the heat transfer performance of SiO<sub>2</sub> nanofluids.

Table 5.  $H$  at different heat flux and  $Re$

Heat Flux, (W/m <sup>2</sup> )	Heat Transfer Coefficient, $h$ (W/m <sup>2</sup> K)				
	$Re = 5000$	$Re = 10000$	$Re = 15000$	$Re = 20000$	$Re = 25000$
6631.5	1769.3	3269.3	4414.7	5511.67	6601.6
7957.8	1769.3	3269.3	4414.7	5511.69	6601.6
9284.0	1769.3	3269.3	4414.7	5511.70	6601.6
26525.8	1769.4	3269.5	4414.9	5511.88	6601.8
53051.7	1769.6	3270.2	4415.3	5512.16	6602.0
79577.5	1769.6	3270.3	4415.4	5512.23	6602.0
106103.3	1769.7	3270.6	4415.7	5512.4	6602.1
132629.1	1769.9	3271.1	4416.0	5512.7	6602.3

The influence of heat flux on the  $\Delta p$  of nanofluids along the tube length at various  $Res$  is shown in Table 6. Generally, the  $\Delta p$  increases when the  $Re$  increases at constant heat flux. The increment of  $\Delta p$  from  $Re$  of 5000 to 25000 for all the heat flux is approximately 2960 kPa. Besides, as the heat flux from the heating coil increases with the condition of a constant  $Re$ , the  $\Delta p$  slightly increases. However, the overall increment of pressure drops is not more than 0.1%. Therefore, the effect of heat flux is negligible when analyzing the  $\Delta p$  in the current simulation.

Table 6.  $\Delta p$  at different heat flux and  $Re$

Heat Flux (W/m <sup>2</sup> )	Pressure Drop, $\Delta P$ (Pa)				
	$Re = 5000$	$Re = 10000$	$Re = 15000$	$Re = 20000$	$Re = 25000$
6631.5	257.3	765.6	1443.1	2237.8	3217.94
7957.8	257.3	765.6	1443.1	2237.9	3217.99
9284.0	257.3	765.6	1443.1	2237.9	3218.03
26525.8	257.3	765.8	1443.5	2238.4	3218.56
53051.7	257.3	766.1	1444.0	2239.1	3219.36
79577.5	257.3	766.2	1444.2	2239.2	3219.57
106103.3	257.3	766.4	1444.6	2239.7	3220.14
132629.1	257.3	766.7	1445.1	2240.4	3220.90

## Conclusion

Forced convective heat transfer and flow performance of SiO<sub>2</sub> nanofluids in turbulent flow along a circular tube is numerically studied. The analysis of the thermal-hydraulic performance found that the  $h$  and  $\Delta p$  are enhanced remarkably when the nanoparticle concentration is increased. The increment in the  $h$  at low  $Re$  and high-volume concentration is around 21.8% while at high  $Re$ , the increment of the  $h$  is about 22.6% which means the higher volume concentration of nanofluids has improved the heat transfer performance. At  $Re$  25000, the increment of  $\Delta p$  from 0% to 1% concentration is only 0.65 kPa while from 3% to 4%, the increment is 1.25 kPa. Besides, there are some non-significant effects of input parameters on heat transfer performance and pressure drop. For instance, the effect of nanoparticle size is relatively small on the  $h$  while the effect of inlet temperature on  $\Delta p$  is also insignificant.

## Acknowledgment

The authors appreciate the financial assistance provided under FRGS/1/2019/TK03/UMP/02/18 from Universiti Malaysia Pahang and the Ministry of Higher Education Malaysia.

## References

- 1) F. Abbas et al., "Nanofluid: Potential evaluation in automotive radiator," *Journal of Molecular Liquids*, 297. 112014, (2020/01/01/ 2020, doi: <https://doi.org/10.1016/j.molliq.2019.112014>).
- 2) P. B. Maheshwary, C. C. Handa, K. R. Nemade, and S. R. Chaudhary, "Role of nanoparticle shape in enhancing the thermal conductivity of nanofluids," *Materials Today: Proceedings*, (2020/01/18/ 2020, doi: <https://doi.org/10.1016/j.matpr.2019.12.315>).
- 3) M. Fares, M. Al-Mayyahi, and M. Al-Saad, "Heat transfer analysis of a shell and tube heat exchanger operated with graphene nanofluids," *Case Studies in Thermal Engineering*, 18. 100584, (2020/04/01/ 2020, doi: <https://doi.org/10.1016/j.csite.2020.100584>).
- 4) S. Mukherjee, P. C. Mishra, and P. Chaudhuri, "Thermo-economic performance analysis of Al<sub>2</sub>O<sub>3</sub>-water nanofluids — an experimental investigation," *Journal of Molecular Liquids*, 299. 112200, (2020/02/01/ 2020, doi: <https://doi.org/10.1016/j.molliq.2019.112200>).
- 5) M. H. Huzaifi, M. A. Budiayanto, and S. J. Sirait, "Study on the carbon emission evaluation in a container port based on energy consumption data," *EVERGREEN Joint Journal of Novel Carbon Resource Sciences & Green Asia Strategy*, 07. (01). 97-103, 2020.
- 6) R. A. Rouf, M. A. H. Khan, K. M. A. Kabir, and B. B. Saha, "Energy management and heat storage for solar adsorption cooling," *EVERGREEN Joint Journal of Novel Carbon Resource Sciences & Green Asia Strategy*, 03. (02). 1-10, 2016.
- 7) M. H. Mahmood, M. Sultan, and T. Miyazaki, "Study on water-vapour adsorption onto polymer and carbon-based adsorbents for airconditioning applications," *EVERGREEN Joint Journal of Novel Carbon Resource Sciences & Green Asia Strategy*, 06. (03). 215-224, 2019.
- 8) D. Li, W. Xie, and W. Fang, "Preparation and properties of copper-oil-based nanofluids," *Nanoscale research letters*, 6. (1). 1-7, 2011.

- 9) K. B. Anoop, T. Sundararajan, and S. K. Das, "Effect of particle size on the convective heat transfer in nanofluid in the developing region," *International Journal of Heat and Mass Transfer*, 52. (9–10). 2189-2195, (4// 2009, doi: <http://doi.org/10.1016/j.ijheatmasstransfer.2007.11.063>).
- 10) A. Ghaffarkhah et al., "On evaluation of thermophysical properties of transformer oil-based nanofluids: A comprehensive modeling and experimental study," *Journal of Molecular Liquids*, 300. 112249, (2020/02/15/ 2020, doi: <https://doi.org/10.1016/j.molliq.2019.112249>).
- 11) S. Suneetha and P. B. A. Reddy, "Investigation on graphene nanofluids and its applications: A brief literature review," *Research J. Pharm. and Tech.*, 9. (6), 2016.
- 12) R. Tadepalli et al., "Characterization of thermophysical properties of Al<sub>2</sub>O<sub>3</sub>, TiO<sub>2</sub>, SiO<sub>2</sub>, sic and CuO nanoparticles at cryogenic temperatures," *Materials Today: Proceedings*, 5. (14, Part 2). 28454-28461, (2018/01/01/ 2018, doi: <https://doi.org/10.1016/j.matpr.2018.10.132>).
- 13) K. Logesh, V. Ramesh, P. B. Thilak Kumar, P. Vijaya Kumar, and B. Akash, "Preparation and property studies of sio<sub>2</sub>/h<sub>2</sub>o nanofluid," *Materials Today: Proceedings*, 18. 4816-4820, (2019/01/01/ 2019, doi: <https://doi.org/10.1016/j.matpr.2019.07.470>).
- 14) A. F. Niwalkar, J. M. Kshirsagar, and K. Kulkarni, "Experimental investigation of heat transfer enhancement in shell and helically coiled tube heat exchanger using sio<sub>2</sub>/ water nanofluids," *Materials Today: Proceedings*, 18. 947-962, (2019/01/01/ 2019, doi: <https://doi.org/10.1016/j.matpr.2019.06.532>).
- 15) C. Jumpholkul, O. Mahian, A. Kasaeian, A. S. Dalkilic, and S. Wongwises, "An experimental study to determine the maximum efficiency index in turbulent flow of sio<sub>2</sub>/water nanofluids," *International Journal of Heat and Mass Transfer*, 112. 1113-1121, (2017/09/01/ 2017, doi: <https://doi.org/10.1016/j.ijheatmasstransfer.2017.05.007>).
- 16) J. Lv, C. Hu, M. Bai, K. Zeng, S. Chang, and D. Gao, "Experimental investigation of free single jet impingement using sio<sub>2</sub>-water nanofluid," *Experimental Thermal and Fluid Science*, 84. 39-46, (2017/06/01/ 2017, doi: <https://doi.org/10.1016/j.expthermflusci.2017.01.010>).
- 17) W. N. Septiadi, K. Astawa, I. G. A. P. Arvikadewi, and D. Febraldo, "Boiling phenomenon of graphene nano-coating wick heat pipe," *EVERGREEN Joint Journal of Novel Carbon Resource Sciences & Green Asia Strategy*, 07, 02. 297-302, 2020.
- 18) S. Hirata and M. Ohtaki, "Simultaneous enhancement in the electrical conductivity and reduction in the lattice thermal conductivity leading to enhanced thermoelectric zt realized by incorporation of metallic nanoparticles into oxide matrix," *EVERGREEN Joint Journal of Novel Carbon Resource Sciences & Green Asia Strategy*, 07. (01). 01-06, 2020.
- 19) J. Al Salami, C. Hu, and K. Hanada, "A study on smoothed particle hydrodynamics for liquid metal flow simulation," *EVERGREEN Joint Journal of Novel Carbon Resource Sciences & Green Asia Strategy*, 06. (03). 190-199, 2019.
- 20) J. Li and C. Kleinstreuer, "Thermal performance of nanofluid flow in microchannels," *International Journal of Heat and Fluid Flow*, 29. (4). 1221-1232, 2008.
- 21) V. Bianco, F. Chiacchio, O. Manca, and S. Nardini, "Numerical investigation of nanofluids forced convection in circular tubes," *Applied Thermal Engineering*, 29. (17–18). 3632-3642, (12// 2009, doi: <http://dx.doi.org/10.1016/j.applthermaleng.2009.06.019>).

- 22) H. A. Mohammed, G. Bhaskaran, N. H. Shuaib, and R. Saidur, "Numerical study of heat transfer enhancement of counter nanofluids flow in rectangular microchannel heat exchanger," *Superlattices and Microstructures*, 50. (3). 215-233, (9// 2011, doi: <http://dx.doi.org/10.1016/j.spmi.2011.06.003>).
- 23) A. Moghadassi, E. Ghomi, and F. Parvizian, "A numerical study of water-based  $\text{Al}_2\text{O}_3$  and  $\text{Al}_2\text{O}_3$ -Cu hybrid nanofluid effect on forced convective heat transfer," *International Journal of Thermal Sciences*, 92. 50-57, (6// 2015, doi: <http://dx.doi.org/10.1016/j.ijthermalsci.2015.01.025>).
- 24) K. Sharma, P. Sarm, W. Azmi, R. Mamat, and K. Kadrigama, "Correlations to predict friction and forced convection  $h$ s of water-based nanofluids for turbulent flow in a tube," *International Journal of Microscale and Nanoscale Thermal and Fluid Transport Phenomena*, 3. (4). 283, 2012.
- 25) P. K. Namburu, D. K. Das, K. M. Tanguturi, and R. S. Vajjha, "Numerical study of turbulent flow and heat transfer characteristics of nanofluids considering variable properties," *International Journal of Thermal Sciences*, 48. (2). 290-302, (2009/02/01/ 2009, doi: <https://doi.org/10.1016/j.ijthermalsci.2008.01.001>).
- 26) A. N. Oumer, James Lau Tze Chen, and A. A. A., "A review on thermo-physical properties of bio, non-bio and hybrid nanofluids," *Journal of Mechanical Engineering and Sciences* 13. (4). 5875-5904, 2019.
- 27) B. C. Pak and Y. I. Cho, "Hydrodynamic and heat transfer study of dispersed fluids with submicron metallic oxide particles," *Experimental Heat Transfer*, 11. (2). 151-170, (1998/04/01 1998, doi: 10.1080/08916159808946559).
- 28) W. Azmi, K. Sharma, P. Sarma, R. Mamat, S. Anuar, and V. D. Rao, "Experimental determination of turbulent forced convection heat transfer and friction factor with  $\text{SiO}_2$  nanofluid," *Experimental Thermal and Fluid Science*, 51. 103-111, 2013.
- 29) F. M. Haghshenas, M. R. Talaie, and S. Nasr, "Numerical and experimental investigation of heat transfer of  $\text{ZnO}$ /water nanofluid in the concentric tube and plate heat exchangers," *Thermal Science*, 15. (1). 183-194, 2011.
- 30) H. Demir, A. S. Dalkilic, N. A. Kürekci, W. Duangthongsuk, and S. Wongwises, "Numerical investigation on the single phase forced convection heat transfer characteristics of  $\text{TiO}_2$  nanofluids in a double-tube counter flow heat exchanger," *International Communications in Heat and Mass Transfer*, 38. (2). 218-228, (2// 2011, doi: <https://doi.org/10.1016/j.icheatmasstransfer.2010.12.009>).
- 31) Y. Xu, M. D. Islam, and N. Kharoua, "Numerical study of winglets vortex generator effects on thermal performance in a circular pipe," *International Journal of Thermal Sciences*, 112. 304-317, (2// 2017, doi: <https://doi.org/10.1016/j.ijthermalsci.2016.10.015>).
- 32) Y. A. Çengel and A. J. Ghajar, "Heat and mass transfer: Fundamentals & applications. McGraw-Hill Education, 2014.
- 33) R. S. Vajjha, D. K. Das, and D. P. Kulkarni, "Development of new correlations for convective heat transfer and friction factor in turbulent regime for nanofluids," *International Journal of Heat and Mass Transfer*, 53. (21-22). 4607-4618, (10// 2010, doi: <http://doi.org/10.1016/j.ijheatmasstransfer.2010.06.032>).
- 34) G. S. Rao, S. KV, S. Chary, B. RA, R. MM, and N. MM, "Experimental study on  $h$  and friction factor of  $\text{Al}_2\text{O}_3$  nanofluid in a packed bed column," *Journal of Mechanical*

Engineering and Sciences (JMES), 1. 1-15, 2011.

- 35) J.-Z. Lin, Y. Xia, and X.-K. Ku, " $\Delta p$  and heat transfer of nanofluid in turbulent pipe flow considering particle coagulation and breakage," *Journal of Heat Transfer*, 136. (11). 111701, 2014.
- 36) W. Duangthongsuk and S. Wongwises, "Measurement of temperature-dependent thermal conductivity and viscosity of tio<sub>2</sub>-water nanofluids," *Experimental Thermal and Fluid Science*, 33. (4). 706-714, (4// 2009, doi: <http://doi.org/10.1016/j.expthermflusci.2009.01.005>).
- 37) S. Mirmasoumi and A. Behzadmehr, "Effect of nanoparticles mean diameter on mixed convection heat transfer of a nanofluid in a horizontal tube," *International Journal of Heat and Fluid Flow*, 29. (2). 557-566, (4// 2008, doi: <http://doi.org/10.1016/j.ijheatfluidflow.2007.11.007>).
- 38) Z. Jia-Fei, L. Zhong-Yang, N. Ming-Jiang, and C. Ke-Fa, "Dependence of nanofluid viscosity on particle size and ph value," *Chinese Physics Letters*, 26. (6). 066202, 2009.
- 39) P. C. Mishra, S. Mukherjee, S. K. Nayak, and A. Panda, "A brief review on viscosity of nanofluids," *International Nano Letters*, journal article 4. (4). 109-120, 2014, doi: [10.1007/s40089-014-0126-3](http://doi.org/10.1007/s40089-014-0126-3).
- 40) V. Trisaksri and S. Wongwises, "Nucleate pool boiling heat transfer of TiO<sub>2</sub>-R141B nanofluids," *International Journal of Heat and Mass Transfer*, 52. (5). 1582-1588, 2009.